micro

MDPI

*Article*

# Updates on an Even More Compact Precision NMR Spectrometer and a Wider Range V-T Probe, for General Purpose NMR and for NMR Cryoporometric Nano- to Micro-Pore Measurements

**John Beausire Wyatt Webber**

Lab-Tools Ltd., Marlowe Innovation Centre, Marlowe Way, Ramsgate CT12 6FA, UK;
dr.beauwebber@gmail.com or nmr@lab-tools.com; Tel.: +44-(0)-7805-437-241

**Abstract:** There is an increasing need for compact low-cost NMR apparatus that can be used on the laboratory bench and in the field. There are four main usage variants of usage: (a) time-domain apparatus, particularly for physical measurements; (b) frequency-domain apparatus, particularly for chemical analysis, (c) NMR Cryoporometry apparatus for measuring pore-size distributions; and (d) MRI apparatus for imaging. For all of these, variable temperature capability may be vital. We have developed compact low-cost apparatus targeted at these applications. We discuss a hand-held NMR Spectrometer, and three different holdable NMR magnets, with sufficiently large internal bores for the Lab-Tools compact Peltier thermo-electric cooled variable-temperature probes. Currently, the NMR Spectrometer is very suitable for (a) NMR time-domain relaxation and (c) NMR Cryoporometry. With a suitable high-homogeneity magnet, it is also appropriate for simple use (b), spectral analysis, or, with a suitable gradient set, (d) MRI. Together, the NMR Spectrometer, one of the NMR variable-temperature probes, and any of these NMR magnets make excellent NMR Cryoporometers, as demonstrated by this paper and previously published research. Equally, they make versatile general-purpose variable-temperature NMR systems for materials science.

**Keywords:** time domain; NMR relaxation; variable temperature; pore size; materials science; Halbach magnet; NMR spectrometer; NMR cryoporometer



**Citation:** Webber, J.B.W. Updates on an Even More Compact Precision NMR Spectrometer and a Wider Range V-T Probe, for General Purpose NMR and for NMR Cryoporometric Nano- to Micro-Pore Measurements. *Micro* **2024**, *4*, 509–529. https://doi.org/10.3390/micro4030032

Academic Editor: Nurettin Sahiner

Received: 30 July 2024
Revised: 3 September 2024
Accepted: 9 September 2024
Published: 13 September 2024



## 1. Introduction

Earlier prototype and preliminary versions of a very compact NMR time-domain NMR Spectrometer (Lab-Tools MK3), with digital R.F. processing and variable-temperature capability, have been presented at the Magnetic Resonance in Porous Media (MRPM) conferences in 2019 [1] and 2022 (in this journal [2]). We will be discussing an even more compact and contained version (Lab-Tools MK4) (think of a 1 lb/500 g tub of butter/spread), with a frequency range up to 50 MHz. A variant, the MK5, is being evaluated, which has an NMR frequency range up to 122 MHz.

We also discuss variable-temperature NMR probes, with an even wider temperature range (−60 °C to +80 °C). These are Peltier thermo-electrically cooled NMR probes suitable for both general-purpose variable-temperature materials-science measurements, and also for NMR Cryoporometric measurements of nano- to micro-scale pore information from porous materials.

We will be presenting recent measurements performed using these instruments, including preliminary experiments on the motional molecular dynamics of ice, in the bulk and in pores, using transverse relaxation time $T_2$ as well as longitudinal relaxation in the rotating frame—the spin-lock $T_{1\rho}$ sequence [3].

Experimental results demonstrate that this compact NMR Spectrometer is capable of working over frequency ranges from sub MHz and up to over 100 MHz. Some groups have been extending the application of this instrument from just the time domain into the frequency domain, at frequencies up to around 100 MHz. Collaborations are underway to

bring full spectroscopy to the MK4 and MK5. Export of NMR Free-Induction Decays (FIDs) to the spectral manipulation and analysis tool MNova [4] is now possible, using standard data formats. Moreover, various groups are applying and extending the multi-nuclear capability of this instrument, which has already been shown to be capable of working with 1H, 19F, 31P, 7Li, 11B and 23Na nuclei.

As well as the current 55 mm Bore 0.3 T Halbach magnet, a more compact 40 mm Bore 0.5 T Halbach magnet is being developed as a more homogeneous replacement for the earlier coffee-mug-sized 36 mm Bore 0.3 T Mandhalas magnet.

## 2. Materials and Methods

The NMR instrumentation described may be grouped as a compatible set of two NMR Spectrometers, a pair of thermo-electrically cooled variable-temperature NMR probes, and a set of three NMR magnets.

### *2.1. MK4 0 to 50 MHz Compact NMR Spectrometer*

The Lab-Tools MK4 NMR Spectrometer for liquids and solids, Figure 1, is primarily a time-domain instrument, being a development of the earlier MK3 design [2], but now has additional software in the Graphical User Interface (GUI) V1.5 Version 5.1.0/7.0 for spectral analysis.

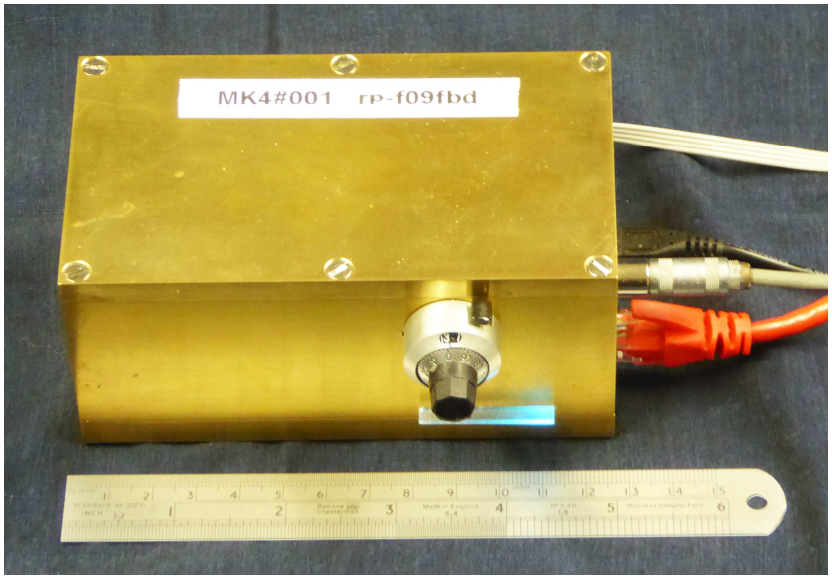


**Figure 1.** The Lab-Tools MK4 compact high-performance NMR time-domain NMR Spectrometer.

The NMR low-noise receiver and NMR linear amplifier that were separate are now combined onto the same printed circuit board (PCB). Additional circuitry that was in the form of external cables with 50 Ohm load and an R.F. attenuator are now also included on the PCB.

The NMR probe tuning capacitor is now also included in the MK4/MK5 boxes. There is a choice of two, the original 1.5 to 40 pF capacitor, or an optional 1.5 to 120 pF capacitor, giving a much wider tuning range.

The same gate-array module as the MK3, the Red Pitaya 125 MHz 14-bit module [5], is used for digital R.F. generation of the NMR pulses and demodulation of the received NMR signal [1,2]. It also has the NMR Pulse Program pipeline that is programmed from a high-level array-processing language (AplX [6,7]) sequence generator in the GUI.

The firmware for this gate array is loaded in a micro-SD card, plugged into the FPGA module. This has additional features compared with the earlier firmware, in that there is additional support for a modified R.F. gate pulse, that allows for damping control at the end of the pulse; see Section 2.1.2.

This module also contains dual 125 MHz 14-bit Digital to Analog converters: OUT1 is used for the RF drive to the NMR linear amplifier; OUT2 can be used under control of the GUI for generation of a low-level constant-amplitude R.F. that can be injected (via the new circuitry) into the NMR receiver circuit. This is used for NMR probe tuning and amplitude calibration.

This module also contains dual 125 MHz 14-bit Analog to Digital receivers: IN1 is used for the reception of the output of the low-noise NMR receiver. IN2 receives a highly attenuated version of the NMR pulse in the NMR probe. This, under control of the GUI, may be used to monitor the amplitude and shape of the R.F. pulse in the probe, and hence may also be used to plot an NMR probe tuning curve.

There is, in addition, a digital output from the gate array that is used to gate the NMR linear amplifier, under control of the firmware, and also a serial output that is used by the menu to fine tune the gain of the low-noise receiver, in conjunction with pins that turn it on and off and switch a 12 dB attenuator on and off.

The AplX software (v1.5) includes a highly effective frequency lock that may be used to lock the NMR Spectrometer frequency to that of the received NMR signal. Even with a fairly broad-band setting, suitable for capturing FID decay signals from ice or polymers, the Spectrometer can follow and lock on to the NMR from a drifting magnet (say from temperature variation) from a liquid signal level of about 1 V, down to a sub 1 mV level, as, say, a sample for NMR Cryoporometry progressively freezes on cooling and then melts again as it is re-warmed up.

### 2.1.1. NMR Graphical User Interface

This is a straightforward development of the GUI for the MK3 NMR Spectrometer [2] (Figure 5); see Figure 2 for a typical example.

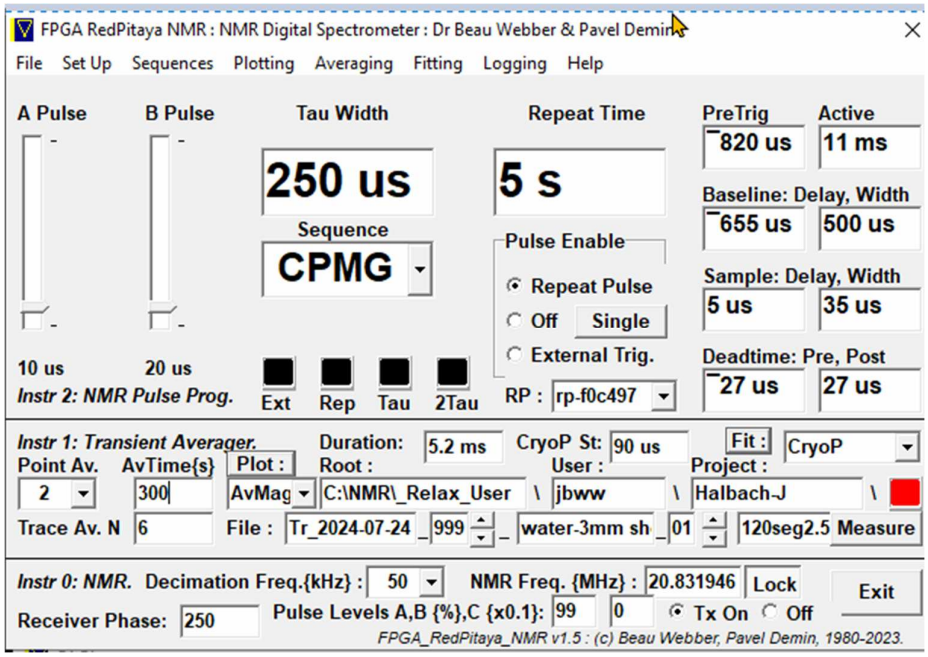


**Figure 2.** A typical Graphical User Interface front panel for a CPMG NMR pulse sequence. It now includes the ability to connect to a range of different MK3, MK4 or MK5 NMR Spectrometers.

There are additional capabilities for frequency-domain plotting, with either Hz or ppm scales, and auto or manual scaling in X or Y; see Figure 3.

The frequency auto-lock can be used to keep the peak fairly well centered, even if the magnet field drifts with temperature.

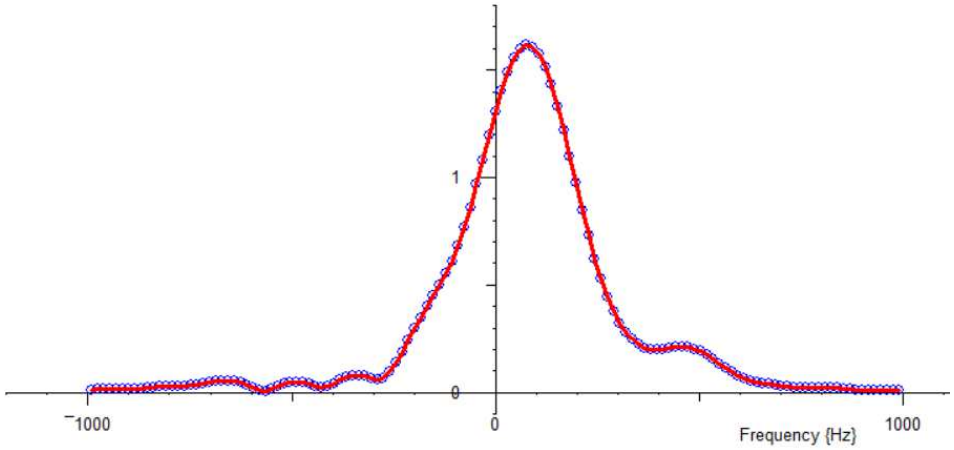


**Figure 3.** Fast Fourier Transform of the first echo in a time-domain signal (the FID can alternatively be transformed). It can be seen that the NMR magnet has slightly changed frequency since the Spectrometer was tuned.

As well as the built-in FFT, the time-domain signal can be exported in standard NMR library formats from the MK4 or Mk5 Spectrometers, enabling import into commercial frequency-domain manipulation and display programs such as MNova [4]; see Figure 4.

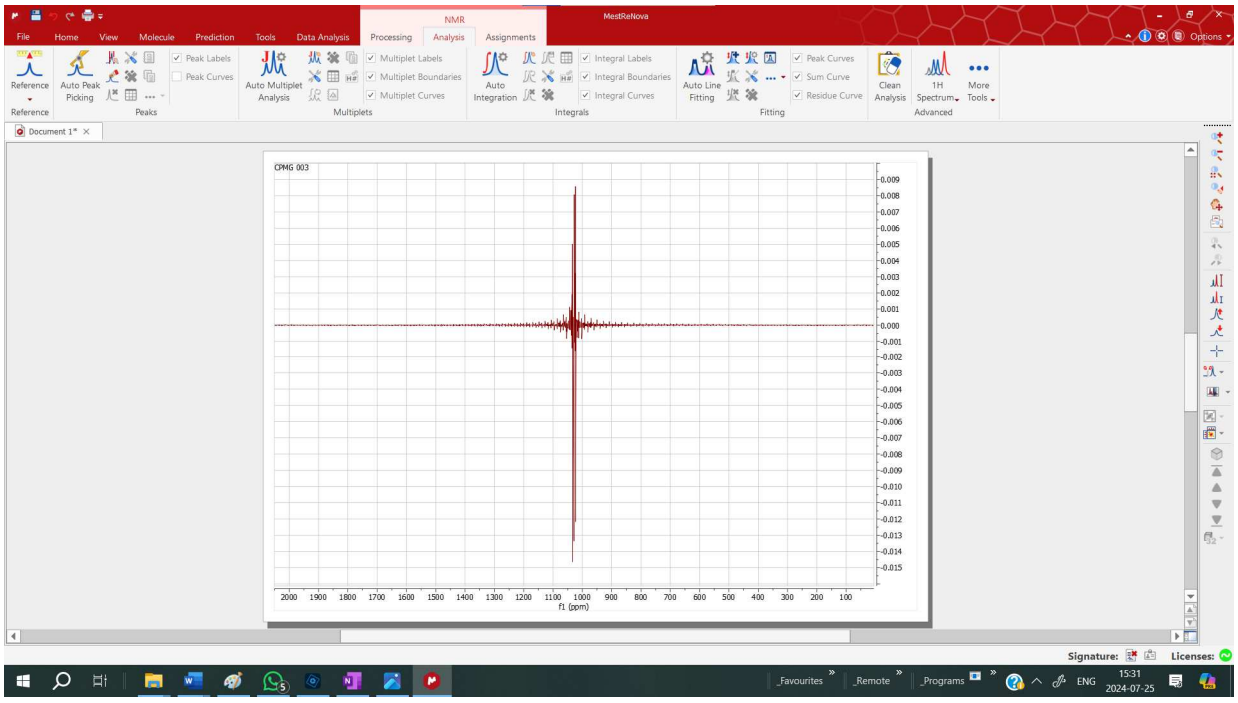


**Figure 4.** An FID and echo captured by an MK4 NMR Spectrometer, exported to and manipulated and displayed by commercial program MNova.

### 2.1.2. NMR Pulse Recovery: Active Damping

When the NMR linear amplifier is enabled by its gate, it amplifies the R.F. input from OUT1 and drives the NMR probe transmitter circuit. When not enabled by its gate, the output goes to a high-impedance state, so as not to damp the NMR probe.

If the amplifier is kept enabled briefly, after the end of the R.F. pulse, it goes into a low-impedance state, and will act to damp the decaying R.F. pulse circulating in the NMR tuned circuit. This brief delay is now settable in the pulse sequence firmware and adjusted in the GUI. Figure 5 shows a briefly damped receiver fast recovery signal.

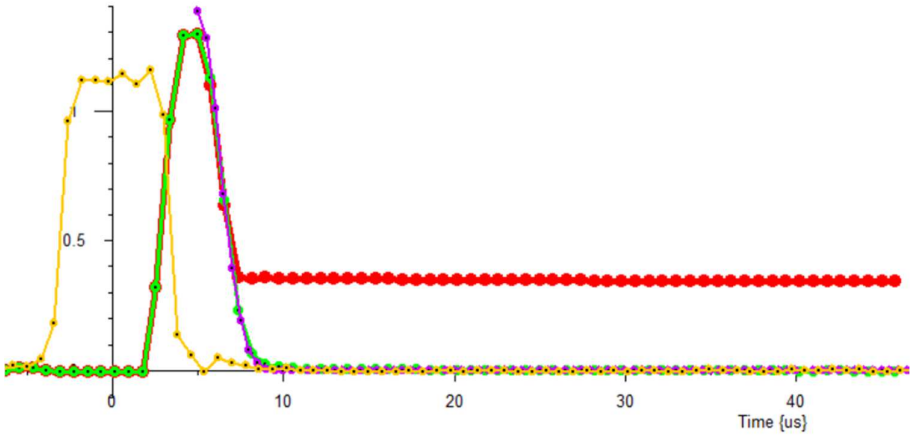


**Figure 5.** With gate set to 2 us: Yellow trace: pulse amplitude; zero time set to middle of pulse. Red trace: water signal with 3-point filter; pulse suppression but no recovery suppression. Green trace: no sample with 3-point filter. Mauve trace: simulated deadtime (5 us from middle of 90 pulses) plus recovery: Gaussian, $T_2$: 1.78 µs.

### *2.2. MK5 0 to 122 MHz Compact NMR Spectrometer*

A development of the Lab-Tools MK4 NMR Spectrometer to a wider frequency range, the MK5, uses a different Red Pitaya gate-array module, the 122.88 MHz 16-bit version [8]. This module contains dual 122.88 MHz 14-bit Digital to Analog converters and 16-bit Analog to Digital converters. The reason for the particular clock frequency chosen is that, expressed in Hertz, it is exactly divisible by two many times, allowing for decimations 1536, 768, 384, 192, 96, and 48. The decimations are used for filtering and receiver data rate reduction.

This version of the Spectrometer operates in two frequency ranges: the first Nyquist zone from 0 to 61 MHz and the second Nyquist zone from 61 to 122 MHz. Currently, external filters are used to assist operation. In the lower frequency range, a 50 MHz low-pass filter removes signal images in the higher Nyquist zones. In the upper frequency range, bandpass filters (say, 10 MHz wide) have been found to work best. A small fixed-gain amplifier block is used to re-amplify the filtered signal to the correct amplitude to drive the linear amplifier.

The NMR receiver and NMR linear amplifier PCB is unchanged from the MK4 version. This has been tested to over 100 MHz; Figure 6 shows a pulse of 90 MHz R.F.

### *2.3. A Range of CryoP Peltier Cooled NMR Probes*

The Peltier thermo-electrically cooled probes have been discussed previously. The first one developed by Lab-Tools was CryoP2, used to cool a 100-Bar pressure probe for gas hydrate research [9].

Current versions are CryoP7, which is a single Peltier device, able to reach around −40 °C or below, and CryoP8, a dual Peltier device, able to reach around −60 °C. Both employ recirculating chillers set at +5 °C coolant temperature, to remove the waste heat. The AplX thermal control software with the Peltiers give extremely stable operation [2] (Section 8), even though the recirculating chillers only have a typical 0.5 °C stability. Both are sized to fit the bores of the Lab-Tools Mandhalas [10] and Halbach [11] NMR magnets.

#### 2.3.1. CryoP7 Peltier Cooled NMR Probe

The CryoP7 Peltier cooled variable-temperature probe is shown in Figure 7, being assembled with an MK4 NMR Spectrometer, and a Halbach J1 NMR Magnet. Also shown is a Pelter cooled recirculating chiller (light enough for mobile use), to remove the waste heat. This variable-temperature probe employs a single Peltier element and digitally controlled power supply, to go down in temperature to about −40 °C, plus a resistance heater and digitally controlled power supply, to also be able to reach +85 °C.

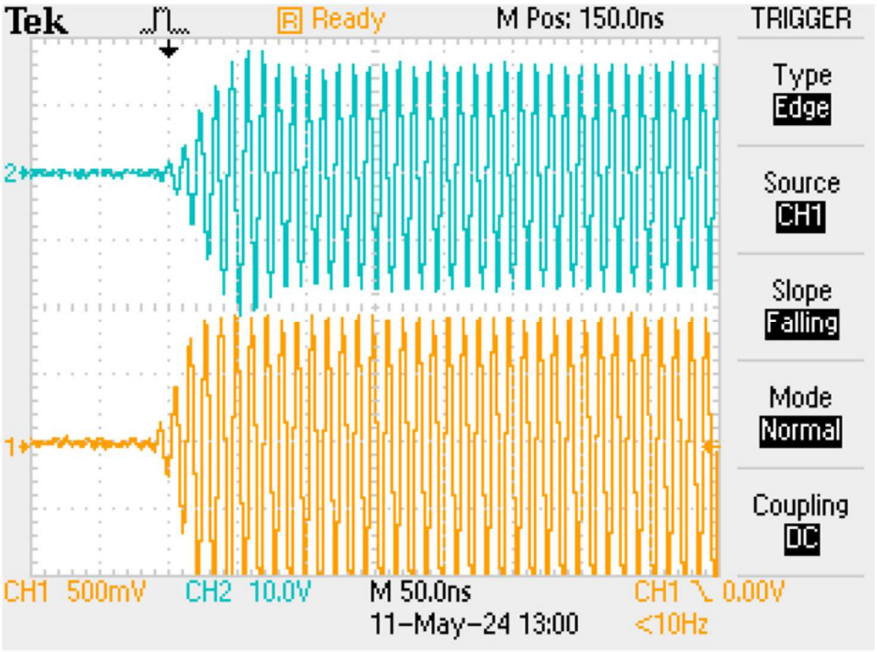


**Figure 6.** A burst of 90 MHz RF; lower trace after the gain block following the band-pass filter, and then at the 50 Ohm input to the NMR linear amplifier; upper trace at the output of the low-impedance NMR linear amplifier.

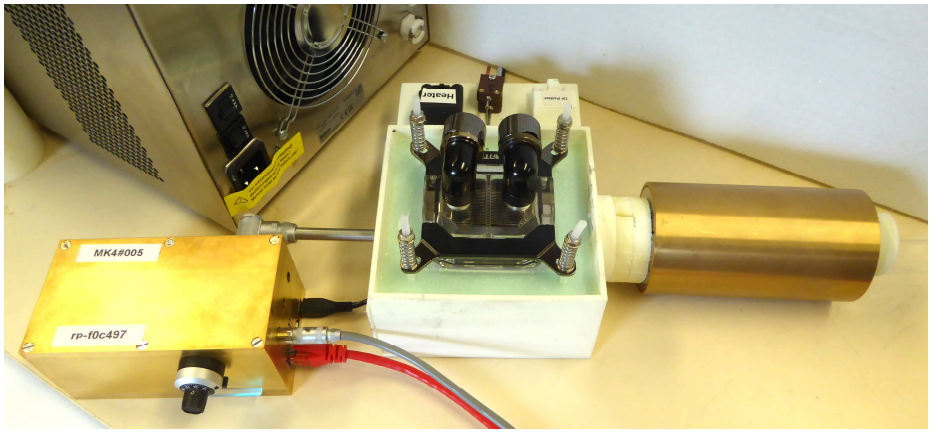


**Figure 7.** CryoP7 Peltier cooled variable-temperature probe with an MK4 NMR Spectrometer and a Halbach J1 NMR Magnet.

Using the technique of NMR Cryoporometry (see Section 3.3), the thermal resolution of these V-T probes (around 10 mK or better, [2] Section 8) enables pore-size distributions up to around a micron in pore diameter to be measured [12]; see Appendix A.

As the temperature decreases, the amplitude of the NMR signal from the sample increases due to the quantum-mechanical spin-population changes—the Boltzmann Effect [11]—and also due to NMR coil resistance changes. When calculating a Cryoporometric melting curve, these changes are corrected for.

In Figure 8, the effect is seen using the CryoP7 Peltier thermo-electrically cooled variable-temperature NMR probe. With a room temperature of 27 °C, the sample temperature is cooled to about −38 °C; with a room temperature of 20 °C, it is cooled to −42 °C.

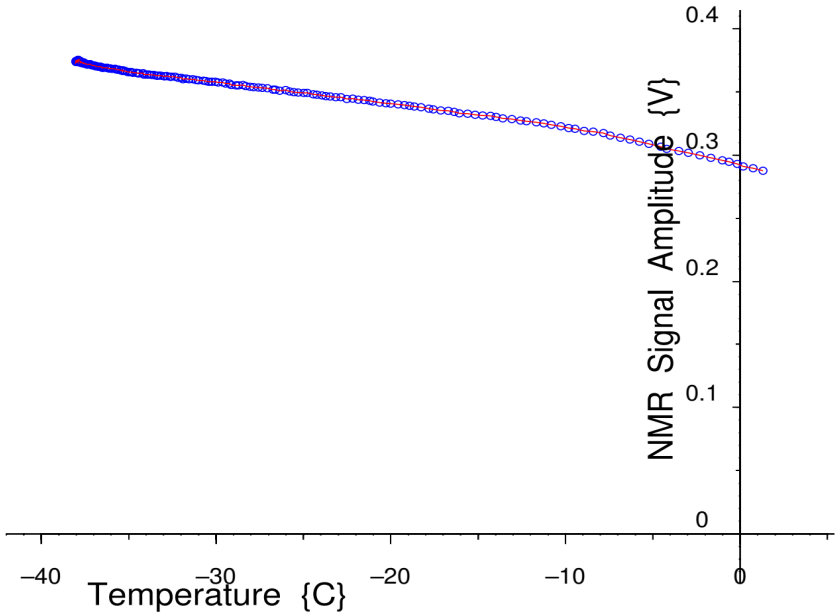


**Figure 8.** A measurement of NMR signal amplitude in a non-freezing sample of hexane, as a function of temperature, in a CryoP7 NMR probe, with room temperature +27 °C.

#### 2.3.2. CryoP8 Peltier Cooled NMR Probe

The CryoP8 Peltier cooled variable-temperature probe is Lab-Tools' latest variable-temperature NMR probe. This variable-temperature probe, like the earlier CryoP6 NMR probe, employs a pair of Peltier elements and two digitally controlled power supplies, to cool down to −57 °C, from an ambient temperature of +20 °C, plus a resistance heater and digitally controlled power supply, to also be able to reach +85 °C.

### *2.4. A Range of Halbach and Mandhalas NMR Magnets*

The Lab-Tools NMR magnets, Figure 9, are all fairly large-bore to enable their use with insulated wide-range variable-temperature NMR probes, or other internal physical or chemical apparatus, including gradient coils.

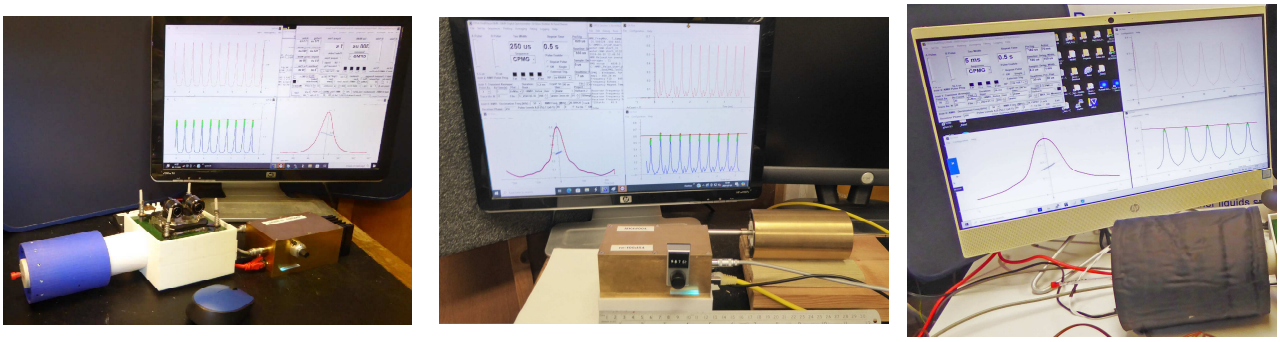

(**a**) (**b**) (**c**)

**Figure 9.** Three different Lab-Tools NMR magnets: (**a**) Blue 0.3 T (12 MHz $^{1}$H) 36 mm ID bore Mandhalas magnet; (**b**) Gold 0.5T (21 MHz $^{1}$H) 40 mm ID bore Halbach J1 magnet; (**c**) Black 0.33 T (14 MHz $^{1}$H) 55 mm ID bore Halbach H magnet (shimmed).

The 36 mm bore Mandhalas M04 [2,10] magnet (Figure 9a) is constructed from 24 individual small cuboid magnets. Work is on-going to shim one of these Mandhalas magnets, to improve the field homogeneity, which, so far, is not good but still fine for CPMG echo trains, as can be seen on the screen in Figure 9a. As a result, it works well for NMR Cryoporometric measurements.

The 40 mm bore Halbach J1 [13] magnet (Figure 9b) is constructed from 8 shaped trapezoidal magnets, and is the highest field magnet of the Lab-Tools set, at 0.5T. When the shimming of the Mandhalas magnet is concluded, the same techniques will be applied to improve the homogeneity of this magnet.

The 55 mm bore Halbach magnet (Figure 9c) is supplied shimmed, and has a good homogeneity for a time-domain magnet, with a $T_2$* of about 5 ms. It should be noted that radiated magnetic fields from bench power supplies may cause phase variations in the NMR signal if they are too close. Working with a magnitude signal (as is commonly carried out for relaxation or Cryoporometry measurements) obviates this problem.

This set of 3 NMR magnets provides a good range of capabilities for compact bench-top and mobile time-domain NMR.

## 3. Results

As well as standard NMR relaxation measurements in liquids, polymers and solids as a function of temperature, this apparatus is capable of more unusual measurements.

### *3.1. NMR Transverse $T_2$ Relaxation Measurements in Solid Brittle Ice*

Very hard solids tend to have short $T_2$ decay times that many NMR Spectrometers find difficult to measure accurately. All the Lab-Tools NMR Spectrometers, MK2, MK3 and now the MK4, have been able to study such samples. Figure 10 shows examples of NMR FIDs in brittle ice, for temperature from −25 °C to −5 °C, measured with an MK4 NMR Spectrometer.

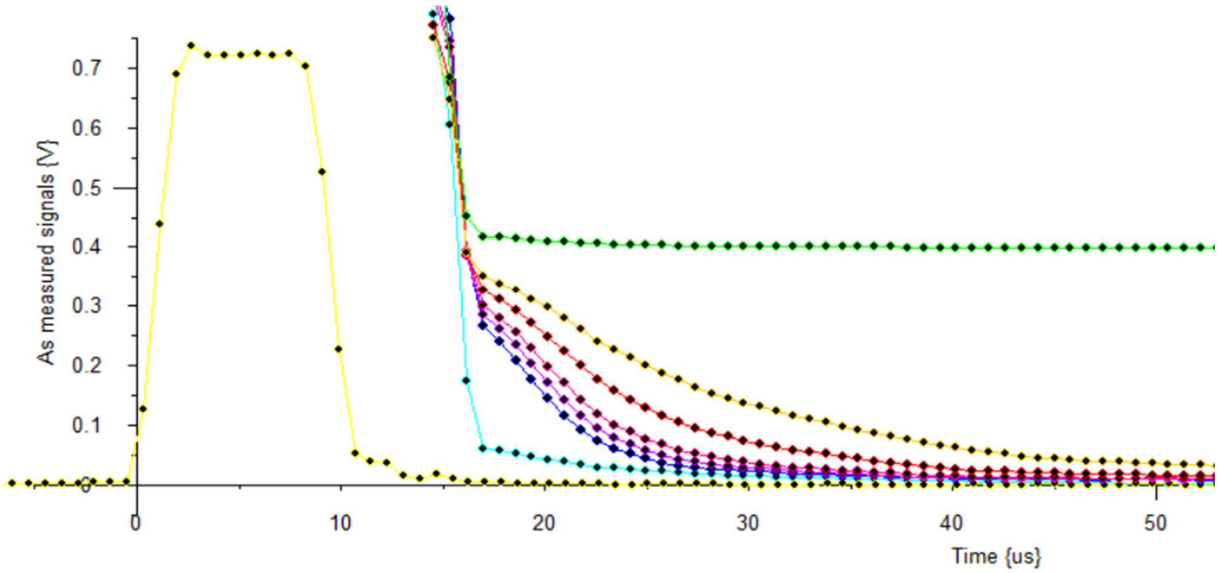


**Figure 10.** Plots: yellow trace: NMR pulse envelope; cyan trace: recovery for empty sample; traces blue to orange: brittle ice at −25 °C, −20 °C, −15 °C, −10 °C, −5 °C; green trace: water at +5 °C. No Boltzmann correction, no baseline correction.

These Spectrometers have been used to study a wide range of solids, polymers and liquids, as well as tars and other hydrocarbons in porous rocks and biochars, as a function of temperature [14].

### *3.2. NMR Longitudinal Relaxation in the Rotating Frame in Water/Ice in Porous Silicas*

NMR longitudinal and transverse relaxation times depend on sample temperature and magnetic field strength, or to be more accurate, NMR frequency. One method of obtaining such data is by measuring in NMR magnets of different $B_0$ field strengths (such as the three Lab-Tools NMR magnets). A much more powerful method is called Fast Field Cycling,

whereby the field $B_0$ of a magnet is rapidly switched from a high value to a lower one, allowing relaxation measurements to be made at a range of NMR frequencies [15].

An alternative method, suitable for lower NMR frequencies, is, following an initial $\pi/2 - x$ NMR pulse, to rapidly apply a continuous R.F. pulse in the $y$ direction. This acts to spin-lock the rotating nuclei for the duration of the pulse, provided that the $B_1$ strength of the rotating field is larger than the local field variations in the sample. By varying the spin-lock duration, $T_1$ in the rotating frame may be measured [3].

There are only a limited number of time-domain NMR spectrometers that are able to measure $T_{1\rho}$ as standard, see Appendix B.

Temperature-dependent minima may often be plotted in the longitudinal relaxation times $T_1$ and $T_{1\rho}$. Figure 11 shows our theoretical curves, for $T_{1\rho}$ field strengths typical for the MK4 NMR Spectrometer, plotted against correlation time $\tau_c$.

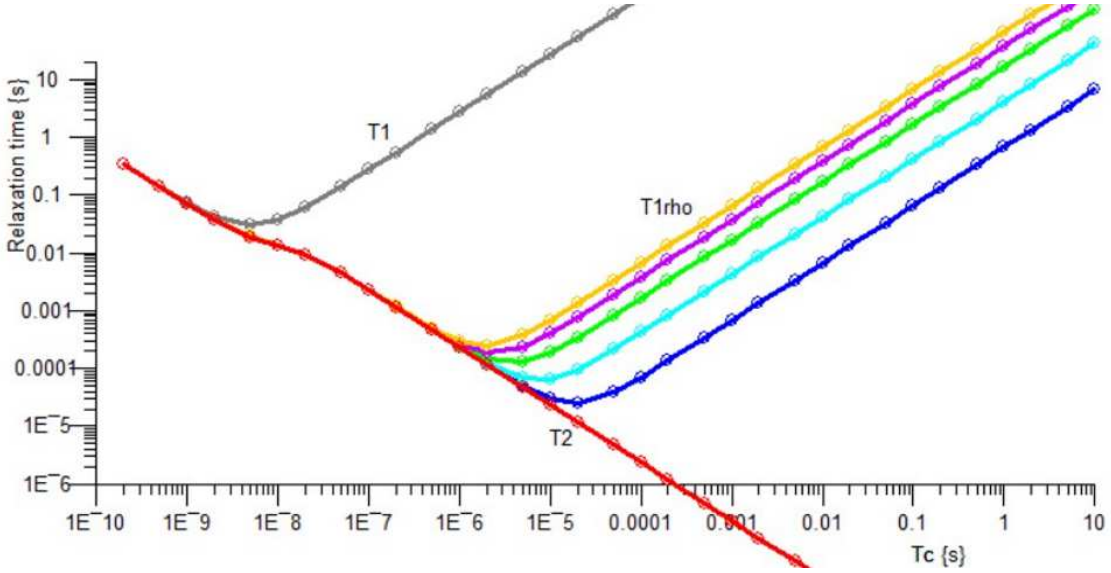


**Figure 11.** Theoretical curves for relaxation times, for $T_1$ transverse relaxation, for $T_{1\rho}$ transverse relaxation in the rotating frame, for $B_1$ field strengths typical for the MK4 NMR Spectrometer, and for $T_2$ longitudinal relaxation, plotted against correlation time $\tau_c$.

The MK4 NMR Spectrometer has been used to measure $T_{1\rho}$ in interfacial ice as a function of temperature, in the pores of a nominal 100Å pore diameter sol–gel silica (Figure 12 and Table 1).

**Table 1.** Parameters for $T_{1\rho}$ powers, $B_1$ fields and rotation rates for the ice in Figure 12.

| Power {%} | B1 {Gauss} | Freq {kHz} | Color |
|---|---|---|---|
| 99 | 5.24 | 22.3 | purple |
| 90 | 4.77 | 20.3 | mauve |
| 80 | 4.23 | 18.0 | orange |
| 70 | 3.71 | 15.8 | yellow |
| 60 | 3.17 | 13.5 | magenta |
| 50 | 2.65 | 11.3 | cyan |
| 40 | 2.11 | 9.0 | blue |
| 30 | 1.6 | 6.8 | green |
| 20 | 1.06 | 4.5 | red |
| 10 | 0.54 | 2.3 | black |

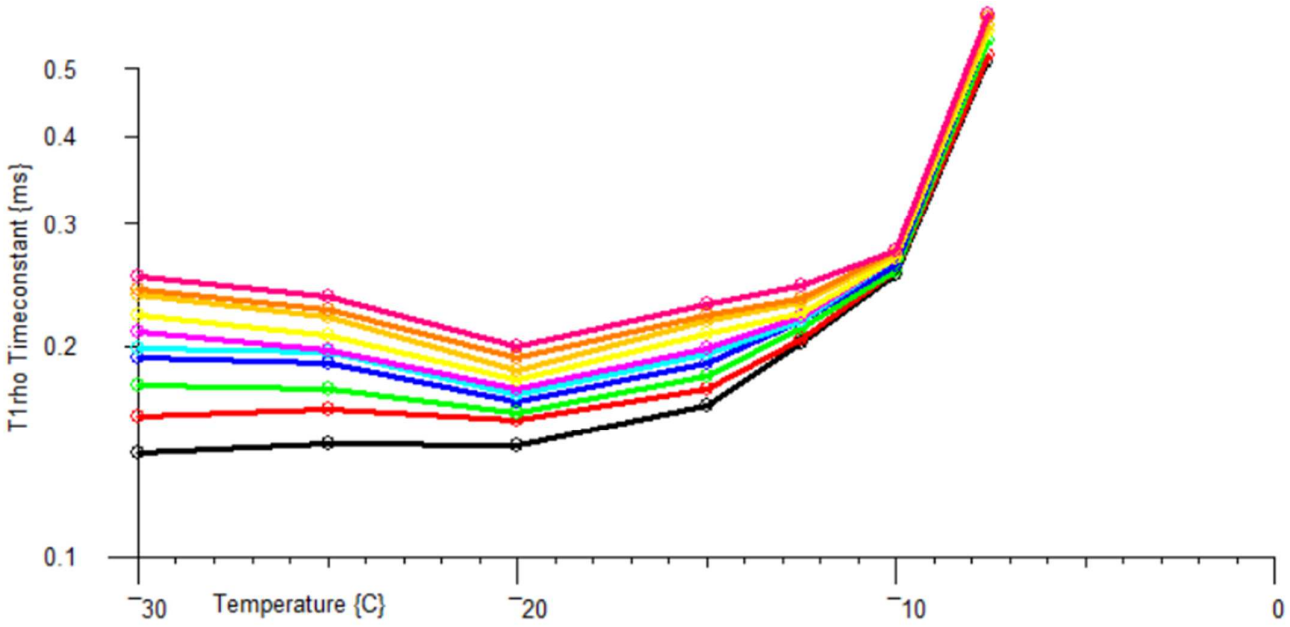


**Figure 12.** $T_{1\rho}$ relaxation time for interfacial ice in a 100Å pore size sol–gel silica. Traces purple to black: rotational frequencies 22 kHz to 2.3 kHz.

These data may also be plotted as a dispersion graph, against rotational frequency, in a form typically used for Fast Field Cycling measurements, as in Figure 13 and Table 2.

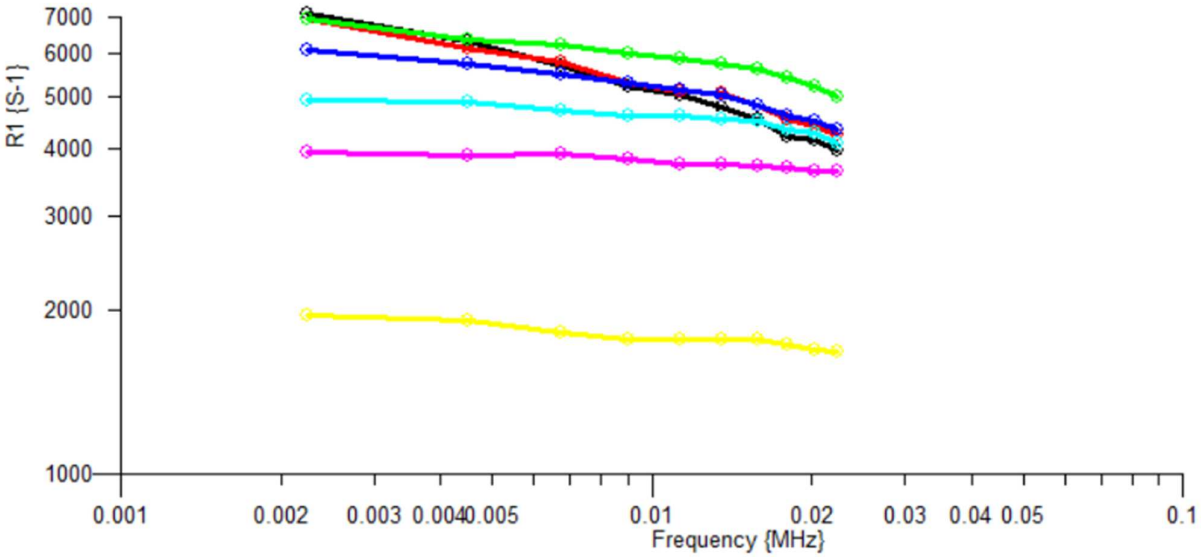


**Figure 13.** These data are plotted as relaxation rate R1, as a sequence of temperatures, on a MHz frequency scale, as is conventional for Fast Field Cycling measurements.

**Table 2.** Temperature parameters for the relaxation rate data in Figure 13.

| Temperature {°C} | Color |
|---|---|
| −30 | black |
| −25 | red |
| −20 | green |
| −15 | blue |

**Table 2.** *Cont.*

| Temperature {°C} | Color |
|---|---|
| −12.5 | cyan |
| −10 | magenta |
| −7.6 | yellow |

### *3.3. NMR Cryopopormetric Measurements Using Water/Ice in a Sol–Gel Silica*

With an MK4 NMR Spectrometer, an earlier CryoP6 V-T probe, and a 55 mm bore 0.33 T Halbach magnet, a vertical-configuration NMR Cryoporometer is shown in Figure 14.

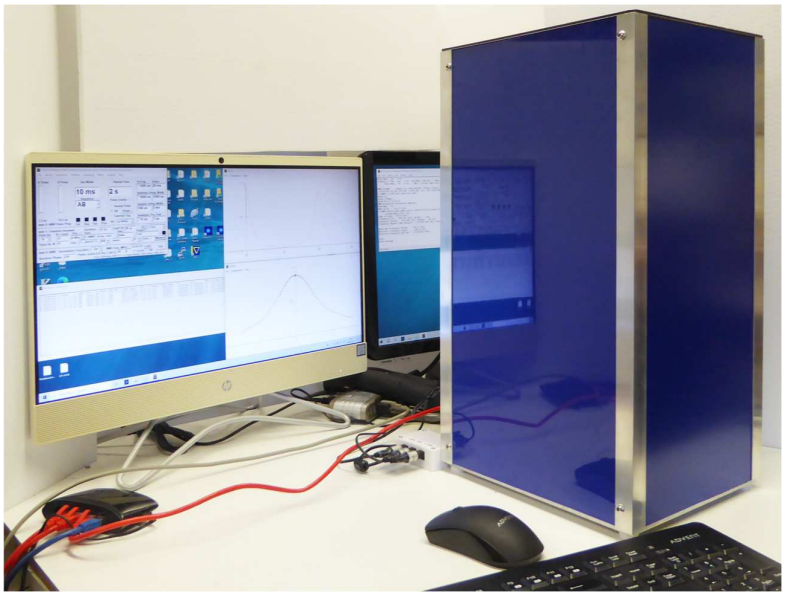

**Figure 14.** An extremely effective variable-temperature NMR system, and NMR Cryoporometer, based on an MK4 NMR Spectrometer, a CryoP6 V-T probe, and a 55 mm bore 0.33 T Halbach magnet, with a dual-screen all-in-one HP computer and monitor.

Figure 15 shows an example warming curve and the corresponding measured pore-size distribution for water in a nominal 100 Å pore sol–gel silica.

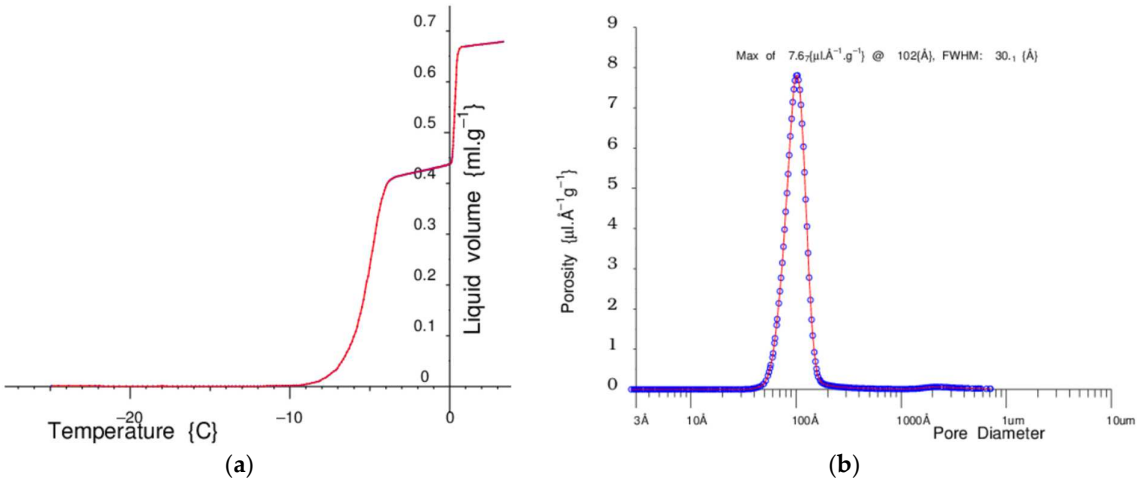


**Figure 15.** (**a**) On the left side is a melting curve, from −25 °C, for water in a sol–gel silica with nominal 100 Å pores. (**b**) On the right is the corresponding pore-size distribution, as calculated from these data, by the Gibbs–Thomson equation.

The sol–gel silica is dried at about 120 °C in an NMR tube and then weighed. A weighed quantity of water is added, just more than enough to fill the pores, and the sample is allowed to equilibrate.

The Pelter thermo-electric device cools the sample down and then very slowly and steadily warms it up. At low temperatures, all the mobile water is frozen solid. As the sample reaches about −8 °C, the ice in the pores starts to melt, until at about −4 °C when all the pore water is melted and there is a plateau. At about 0 °C, the bulk liquid outside the grains starts to melt, and then there is a final plateau.

Standard NMR Cryoporometric theory [16–19] may then be applied to deduce a pore-size distribution; see Appendix A.

### *3.4. Mobile NMR Measurments in the Field—Water and Oil Content of Seeds*

A Lab-Tools MK4 spectrometer and 0.5 T Halbach magnet were set up in the field, with an 8 h regulated battery supply (in the black bag), together with a laptop for control, analysis and display, Figure 16. A set of transverse $T_2$ relaxation measurements were then made using CPMG pulse sequences, on two types of seed:

Linseed—golden, and Sesame—white.

5 seeds of each type were added to 3 mm NMR tubes, (5 mm tubes could have been used).

Linseed—golden: 21.4 mg.

Sesame—white: 14.2 mg.

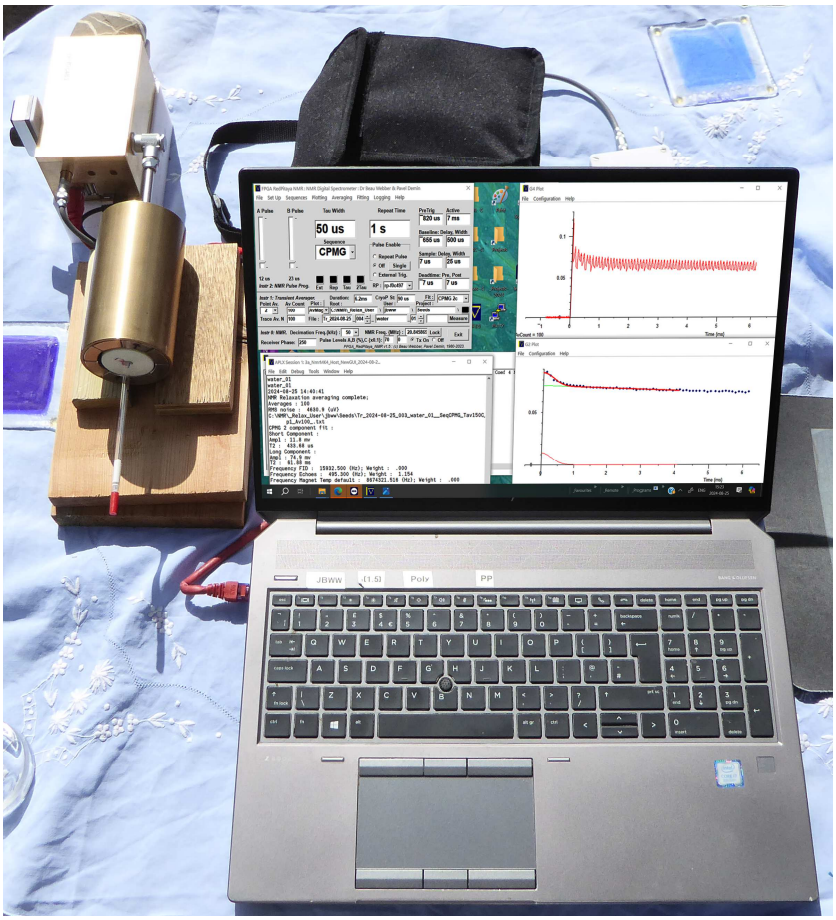


**Figure 16.** MK4 NMR Spectrometer and Halbach J1 Magnet—top left, 8 h regulated battery supply behind laptop.

The data was measured for 100 s each, and then fitted using selected routines. Both sets of data were clearly 2 component, Figure 17, (no further components were seen to

100 ms). Literature shows that the small short decays are water, the larger long decays are the oil in the seeds.

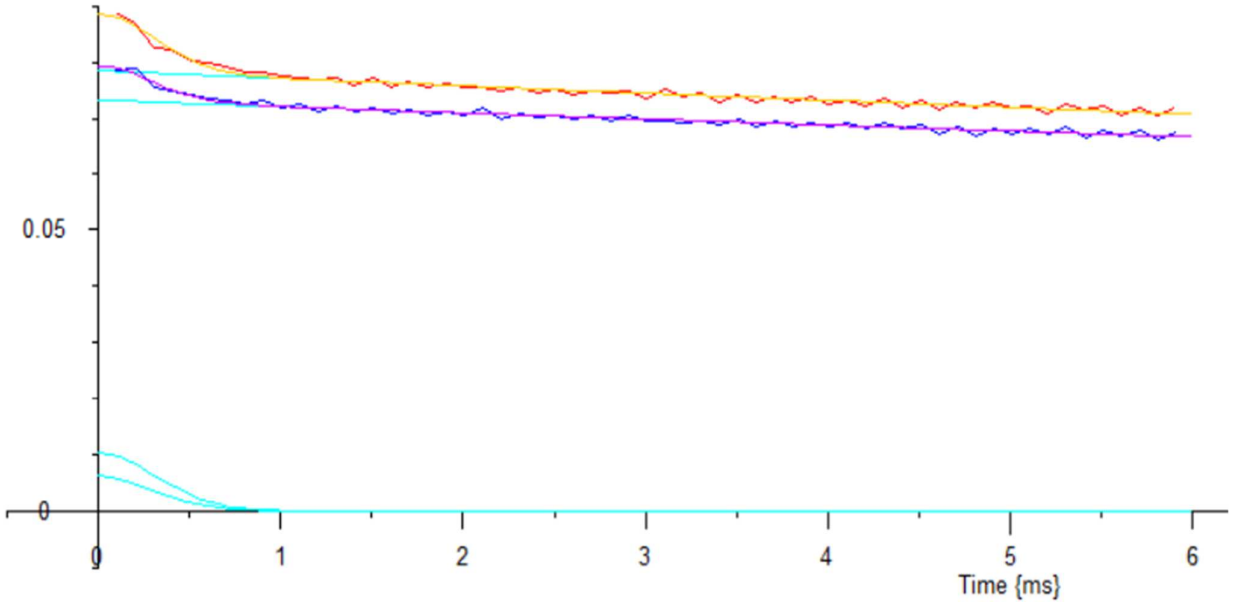


**Figure 17.** The upper red trace is the measured CPMG $T_2$ decay from the 5 linseeds; the yellow line through it is a Gaussian-exponential fit, which is decomposed into the upper long cyan decay, and the upper short Gaussian cyan decay. The dark blue trace is the measured CPMG $T_2$ decay from the 5 sesame seeds; the mauve line through it is also a Gaussian-exponential fit, which is similarly decomposed into two further cyan lines. Vertical scale measured in Volts.

The measured components were as follows:
**Linseed—Golden:**
CPMG 2-component fit:
Short Component:
Ampl: 10.2 mv;
T2: 441.63 µs.
Long Component:
Ampl: 78.5 mv;
T2: 57.71 ms.
**Sesame Seed—White:**
CPMG 2 component fit:
Short Component:
Ampl: 6.1 mv;
T2: 413.91 us.
Long Component:
Ampl: 73.3 mv;
T2: 63.93 ms.

It should perhaps be noted that these fitted data and the graphs were available immediately at the end of each averaging measurement.

And yes it did rain briefly!

### *3.5. Example Measurements of Fluorine Chemically Resolved Spectra: $^{19}$F Spectra Using the Lab-Tools MK4 NMR Spectrometer and a 0.33T Shimmed Halbach Magnet*

Measured NMR FIDs may be transformed to spectra [20]. Spectrally resolved NMR requires good homogeneity magnets, and $^{1}$H spectra have been beyond the capabilities of our current NMR magnets. However, $^{19}$F Fluorine-based chemicals have wide-range spectra, enabling chemically resolved spectra in lower homogeneity NMR magnets.

Here, we have made some measurements on hexaflurobenzene and octaflurotoluene, and on two mixtures of hexaflurobenzene and octaflurotoluene. The samples were about 10 mm long, in 3 mm NMR tubes (2.5 mm ID). FIDs were measured with an MK4 NMR Spectrometer in our 0.33 T Halbach magnet. Complex captured data of length $2^n$ points were processed with a $\cos^2$ window function, and four-fold zero-padding, followed by a Fast Fourier Transform (FFT).

The FID for the hesaflurobenzene was a smooth decay, as expected for the all-equivalent $^{19}$F atoms. In the absence of any other spectral reference, the NMR Spectrometer was locked to this signal.

The FID for the Octaflurotolune showed a beating structure, as expected for the two non-equivalent $^{19}$F atoms. With the Spectrometer set 5 kHz off the signal lock frequency, the following FID (Figure 18a) and spectrum were obtained after 30 s averaging.

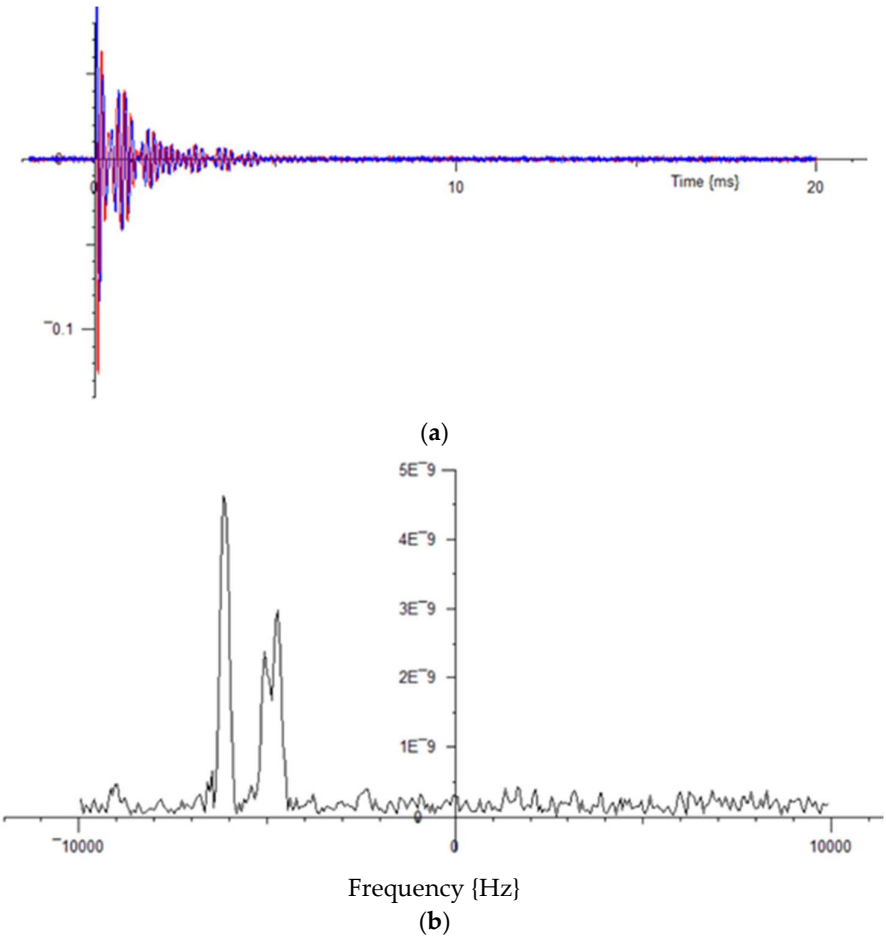


**Figure 18.** (**a**) (Upper) NMR FID for Octaflurotolune, with the Spectrometer set 5 kHz off the signal lock frequency. (**b**) Transformed Fourier data, from 30 s averaging. These have been deliberately taken directly from the screen, as an example of the immediately available display.

In the preparation for Figure 19 using mixtures of hexaflurobenzene and octaflurotoluene, the adding of extra octaflurotoluene to mixture A, to obtain mixture B, clearly demnstrated that the Octaflurotolune gives rise to the two smaller peaks, as expected. These data may be exported from the GUI to spectral processors—i.e., Mnova [21].

The resolution was limited by both the magnetic field variation over the sample and, in particular, by the field drift during the measurement. The spectra here were all averaged for only 30 s in the time domain, to reduce this problem.

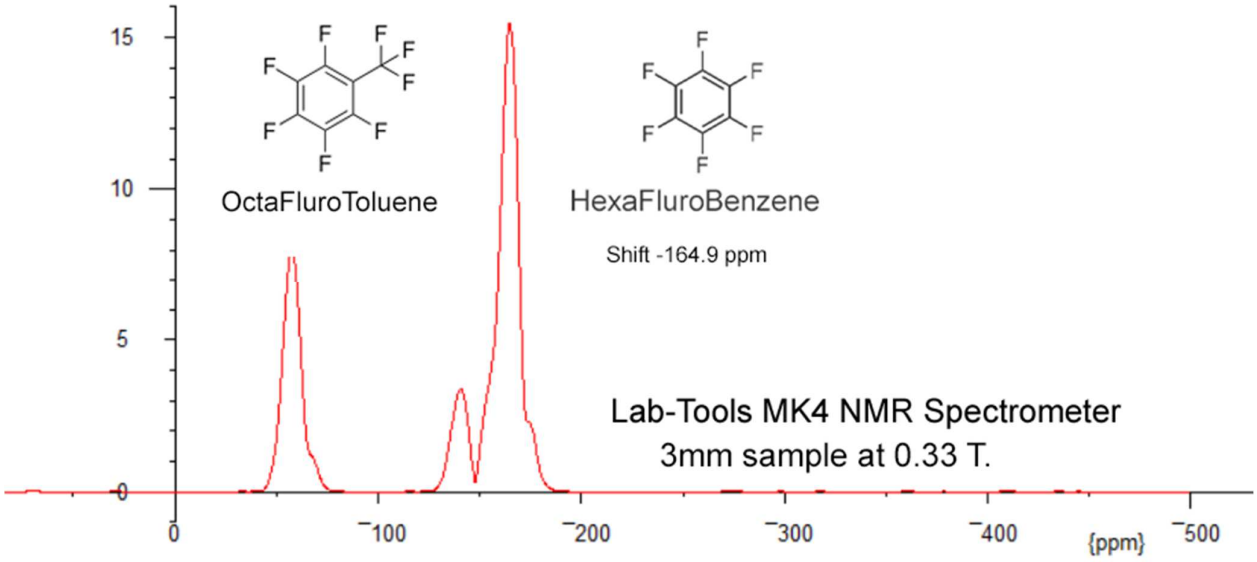


**Figure 19.** Spectra for mixture B (with addded octaflurotoluene). These data are the average of a number of separate 30 s captures and FFTs, plus aligning all the main hexaflurobenzene peaks to the literature ppm shift of −146.9 ppm.

A preliminary investigation was carried out on the practicality of measuring $^{19}$F spectra over a wide temperature range. Mixture B spectra were successfully measured from about −50 °C to +50 °C, at about 0.5 °C steps. Over this temperature range, the peak amplitudes changed by a factor of about three. However, as expected, Boltzmann and coil resistance corrections to a common 0 °C reduced this variation to a moderate residual scatter, Figure 20b.

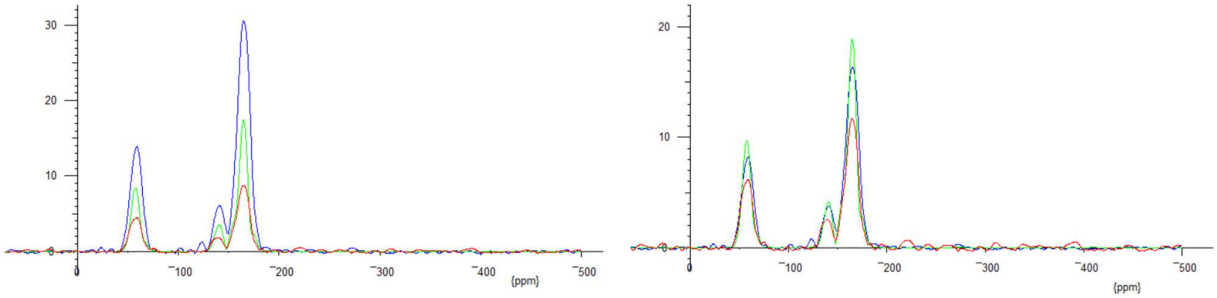


(**a**) (**b**)

**Figure 20.** (**a**): Three spectra from mixture B: Blue −48 °C, Green +26 °C, Red: +45 °C. (**b**) after Boltsmann and copper coil resistance corrected to 0 °C; Blue −48 °C, Green +26 °C, Red: +45 °C.

This demonstrates the suitability of this apparatus for following chemical processes over a wide temerature range. The Lab-Tools 2 to 122 MHz MK5 NMR Spectrometer is also of great help for better spectral resolution, in, for example, suitable 2 T Magnets, and two other groups are working towards benchtop $^{1}$H spectra with MK5 Spectrometers.

### *3.6. NMR Imaging Protocol Combined with NMR Cryoporometric Protocol*

The measurement of an NMR FID in the presence of a magnetic gradient enables the creation of NMR images by the application of Fourier Transforms [22]. The above Halbach NMR magnets have good internal room for gradient coils, although to date, these have not yet been designed or purchased for use with the MK4 NMR Spectrometer.

However, as an example of work we wish to continue, prior work was undertaken with the earlier MK2 NMR Spectrometer, combining 1D imaging and Cryoporometric protocols [17] is shown in Figure 21.

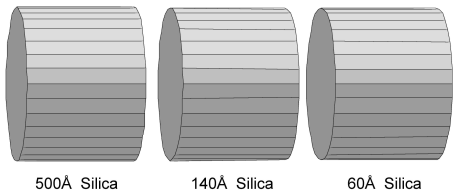


*(a:) 1D porous silica phantom with axial structure in the y direction.*

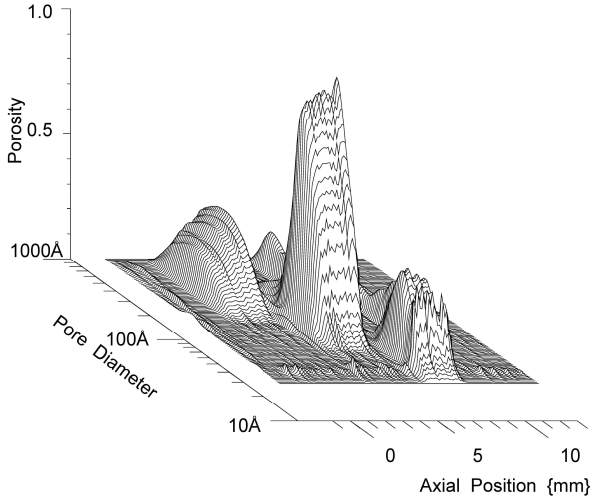


*(b:) 1D resolved porosity for 3 part phantom.*

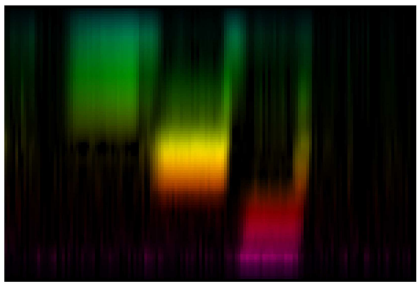

*(c:) Colour map of Pore Size.*

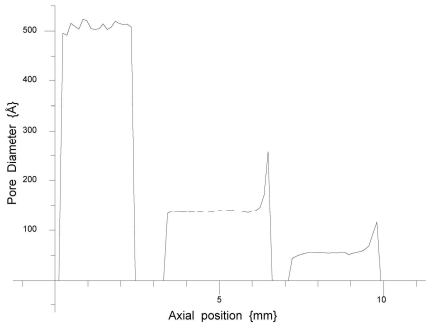


*(d:) Median pore size as a function of axial position, for the phantom constructed from nominal 500Å, 140Å and 60Å silicas.*

**Figure 21.** A sample consisting of three different pore size sol-gel silicas was prepared, and a liquid (water or cyclohexane) added to the sample. It was placed in an axial magnetic gradient, to enable a 1D imaging protocol to be applied. This sample was then cooled down until all the liquid was frozen, and then slowly warmed. This progressively melted the liquids in the different pore sizes, enabling a NMR Cryoporometric protocol to be applied [23]. In the colour map, blue-green is highest, then yellow, and red the smallest pore-size. (**a**) shows a schematic of a linear three part sol-gel sample, constructed with a 60 Å pore-size section, a 140 Å section, and a 500 Å section, all separated by Teflon spacers. A probe liquid was added to the porous silicas, either water or Cyclohexane. A linear magnetic field gradient was applied from a coil and power supply, to provide an MRI encodisng protocol of axial position. This sample was then cooled down until all the liquid was frozen, and then slowly warmed. This progressively melted the liquids in the different pore sizes, enabling a NMR Cryoporometric protocol to also be applied [23]. (**b**) shows a 3 dimensional plot, that is effectively a pore-size distribution graph of Porosity vs Pore Diameter, for each of the set of available axial positions. (**c**) shows this information as a colour map, blue-green is highest, then yellow, and red the smallest pore-size; (**d**) plots a graph of median pore-size, vs axial position, which well resolves the three pore sizes.

Later work continued to focus on other NMR Spectrometers and magnets, to combine NMR Cryoporometry with 2D and 3D imaging protocols [24]. With an appropriate magnetic field gradient system, the MK4 Spectrometer and Halbach magnets should be able to continue this work.

### *3.7. Summary*

NMR apparatus suitable for mobile use in the field has been demonstrated, and also for measurement of $^{19}$F chemically resolved spectra.

These sections have demonstrated low-cost but precise apparatus suitable for wide-range temperature measurement, including the most effective NMR Cryoporometer of this series to date. The range offers various size and cost options. This result is particularly clean in terms of NMR signal-to-noise, and a precise, well-resolved resultant pore-size distribution is obtained. Measurements from sub-nanometer to about 2-micron pore diameters have been obtained using earlier versions of these NMR Cryoporometers [12,25,26]. These variable-temperature NMR/NMRC systems are now used regularly by various national and international organizations.

We look forward to re-instating the ability to measure magnetic field gradients, so as to measure spatially resolved images and continue prior work on spatially resolved NMR Cryoporometry.

## 4. Discussion

This paper discusses the successful development of a progressive range of low-cost compact bench-top and mobile apparatus to facilitate NMR studies for materials science.

Prior work using MK2 and Mk3 NMR Spectrometers has resulted in the writing of over 50 papers, often with joint international authors [17], exploring the properties of a wide range of materials. These have included sol–gel silica, templated silicas and MOFs [12,25], porous rocks [14], biochar and other porous carbon material [14], nano-interface materials for batteries [26], porous meteorites [27], biological materials [28] and melanin from date palms [29].

Future work will involve further exploring the smallest and largest nano- to micro-pores that can be successfully and repeatably resolved using NMR Cryoporometry, using these latest CryoP7 and CryoP8 Peltier thermo-electrically cooled NMR probes.

Further work on improving the homogeneity of the Mandhalas and Halbach NMR magnets is underway, at least certainly for time-domain relaxation studies, but also targeting low-resolution $^{1}$H spectral studies. This capability will offer the ability to monitor the evolution of chemical processes with time and temperature.

The spectral resolution of at least simple $^{1}$H organic molecules is a desirable goal, to enable chemical process monitoring. This requires considerable improvements in magnet homogeneity, but measuring the chemical resolution of $^{19}$F organic molecules has now been demonstrated.

## 5. Patents

Webber, J.B.W. Nuclear Magnetic Resonance Probes. U.S. Patent 9,810,750 B2, 7th November 2017.

**Funding:** This research received no external funding.

**Institutional Review Board Statement:** Not applicable.

**Informed Consent Statement:** No research involving humans.

**Data Availability Statement:** No additional data.

**Acknowledgments:** The author would like to thank Pavel Demin for his development of the excellent firmware used in the gate array.

**Conflicts of Interest:** The author declares no conflicts of interest.

## Appendix A

### *Appendix A.1. NMR Cryoporometry (NMRC) Theory*

Josiah Willard Gibbs and three different Thomsons (James Thomson, William Thomson (later Lord Kelvin) and J.J. Thomson) applied experiment, thermodynamics and generalized dynamics to produce an equation that well describes the phase-change behavior of liquids in confined geometry; the Gibbs–Thomson equation for the melting point depression, $T_m$, for a small isolated spherical crystal, of diameter $x$, in its own liquid, may be expressed as [16,17]

$$\Delta T_m = T_m^{\infty} - T_m(x) = 4\sigma_{sl} T_m^{\infty} / x \Delta H_f \rho_s. \quad \text{(A1)}$$

A development of the Gibbs–Thomson equation has been discussed that relates these phase changes so that the pore area $a_p$ and volume $v_p$ are related to the melting point depression [16,17]:

$$\Delta T_m = T_m - T_m(x) \approx \frac{a_p}{v_p} \cdot \frac{\sigma_{sl} T_m \cos(\varphi)}{\Delta H_f \rho_s} \approx \frac{k_d \sigma_{sl} T_m}{x \Delta H_f \rho_s}. \quad \text{(A2)}$$

For many purposes, this may be simplified so that the pore diameter $x$ is related to a melting point depression {K} = $T_m = k_{GT}/x$, where we are grouping all the thermodynamic terms into a single constant, $k_{GT}$ {K.Å}—the Gibbs-Thomson coefficient—usually established by experiment [16,17], and then applied; see Figure 15.

It is important to note that $k_{GT}$ includes a term dependent on pore geometry, as does the Kelvin equation. $k_d$ is the geometry term and is equal to four for a spherical liquid–crystalline interface (conventionally assumed for cylindrical pores). $T_m$ is the bulk melting point and the other terms are thermodynamic and density terms.

Thus, the transformation of melting-point depression to pore size is given by the Gibbs–Thomson equation, while the measurement of the pore volume vs. size distributions is facilitated by differentiating and re-mapping the melting curve data using the Strange–Rahman–Smith transformation:

$$\frac{dv}{dx} = \frac{k_{GT}}{x^2} \cdot \frac{dv}{dT}. \quad \text{(A3)}$$

The Strange–Rahman–Smith equation transforms the quantity of liquid measured at any particular temperature to an incremental pore volume as a function of pore size.

### *Appendix A.2. Practical Applications and Limitations*

Common liquids used for NMR Cryoporometry probes include water, cyclohexane, and n-alkanes that melt around room temperature. We have determined the $k_{GT}$ coefficients for most of these. Thus, for water, a temperature of around $-60$ °C is required to reach a lower pore size of around 1 nm.

For a pore-size resolution in the micron range, a temperature resolution of around 10 mK is required, as has been demonstrated [2] (Section 8) [12]. The use of cyclohexane as the probe liquid, for instance, can extend this range up in pore size by a further factor of three.

In Figure A1, the pore-size distribitions in two bi-modal porous silicon oxide samples were measured using hexadecane as the probe liquid. The total volume of macropores (from 50 Å to 3 nm) predominated over the mesopores (20–500 Å), even though the peak porosity of the latter is higher [12]. Hexadecane also has a larger $k_{GT}$ than water, about 1000 Å.K, which facilitates this micron pore-size measurement.

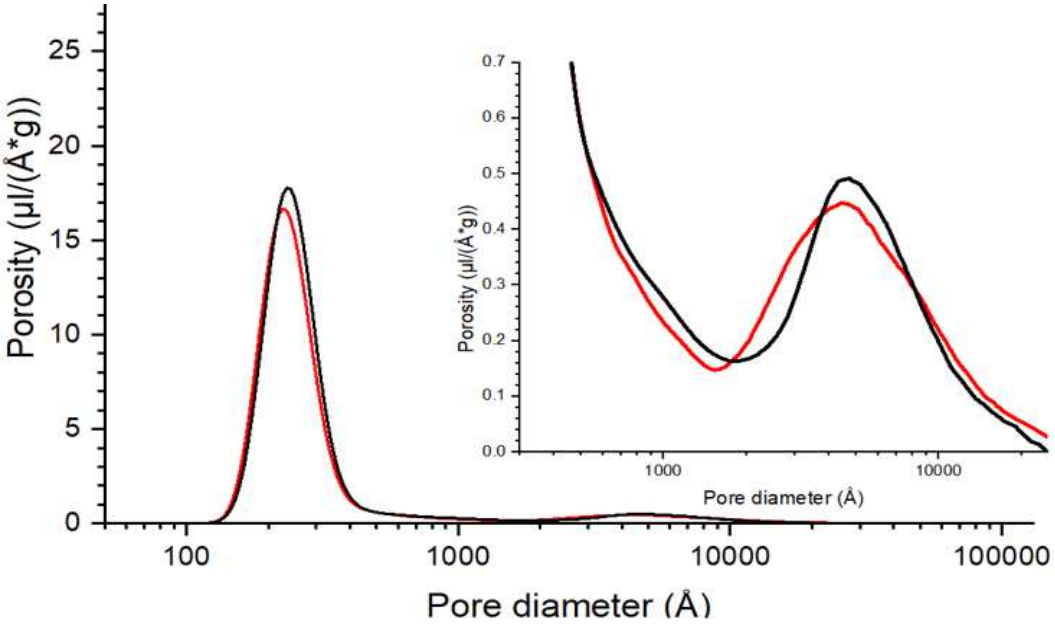


**Figure A1.** The pore-size distribitions in two bi-modal porous silicon oxide samples were measured, using hexadecane as the probe liquid. The total volume of macropores (from 50 Å to 3 nm) predominated over the mesopores (20–500 Å) [12].

## Appendix B

The following NMR instrument suppliers responded to our requests for further information on their Time-Domain NMR spectrometers. All these instruments, with the exception of Turbospec, appear to offer reasonably wide-range sample temperature control.

All these instruments, with the exception of Turbospec, can study rigid solids and solid polymers, as well as liquids.

### *Appendix B.1. Comparable Table-Top Time-Domain NMR Instruments*

Bruker, Coventry, UK—Minispec—to 60 MHz—inc T1$\rho$ [30]
Oxford Instruments, High Wycombe, UK—MQC+—to 23 MHz [31]
Resonance Systems, Kirchheim, Germany—Spin Track—to 80 MHz—inc T1$\rho$ [32]
Turbospec LLC, San Diego, CA, USA—Turbospec—e400 [33]
Lab-Tools Ltd., Ramsgate, UK—MK4—to 50 MHz—inc T1$\rho$ [34]
Lab-Tools Ltd.—MK5—to 122 MHz—inc T1$\rho$ [34]

### *Appendix B.2. Floor-Standing Time-Domain NMR Instruments*

Oxford Instruments—MQR—20 MHz—inc T1$\rho$ [35]
Oxford Instruments—GeoSpec 2—2 MHz [36]
Oxford Instruments—GeoSpec 12—12 MHz [36]
LexMar Global Inc., Haverhill, MA, USA—Mag Station—20 MHz [37]
LexMar Global Inc.—MagModule—20 MHz [38]
Stelar s.r.l, Mede (PV), Italy—SMARtracer—FFC NMR relaxometer—inc T1$\rho$ [39]

## References

1. Webber, J.B.W.; Demin, P. Credit-card sized field and benchtop nmr relaxometers using field programmable gate arrays. *Magn. Reson. Imaging* **2019**, *56*, 45–51. [CrossRef] [PubMed]
2. Webber, J.B.W.; Demin, P. Digitally based precision time-domain spectrometer for nmr relaxation and nmr cryoporometry. *Micro* **2023**, *3*, 404–433. [CrossRef]
3. Redfield, A.G. Nuclear magnetic resonance saturation and rotary saturation in solids. *Phys. Rev.* **1955**, *98*, 1787–1809. [CrossRef]
4. Cobas, J.C.; Sardina, F.J. Nuclear magnetic resonance data processing. mestre-c: A software package for desktop computers. *Concepts Magn. Reson. Part A* **2003**, *19*, 80–96. [CrossRef]

5. Pitaya, R. *Stemlab 125-14*; Red pitaya: Solkan, Slovenia, 2013; Available online: https://redpitaya.com/stemlab-125-14/ (accessed on 5 September 2024).
6. Iverson, K. *A Programming Language*; Wiley: New York, NY, USA, 1962.
7. Nabavi, R. *Microapl: Aplx, micoApl's AplX Interpreter, version*; MicroAPL Ltd.: East Sussex, UK, 2007; Available online: http://www.microapl.co.uk/APL/ (accessed on 5 September 2024).
8. Pitaya, R. *Sdrlab 122-16*; Red pitaya: Solkan, Slovenia, 2020; Available online: https://redpitaya.com/sdrlab-122-16/ (accessed on 5 September 2024).
9. UK Research and Innovation. Grant: EPSRC.; EP/d052556/1: Capillary Controls on Gas Hydrate Growth and Dissociation in Synthetic and Natural Porous Media: PVT, NMR, Neutron Diffraction and SANS. Available online: https://gtr.ukri.org/project/8129FC4B-D0BB-40B6-9810-CFF01EA935FC (accessed on 5 September 2024).
10. Raich, H.; Blümler, P. Design and construction of a dipolar halbach array with a homogeneous field from identical bar magnets: NMR Mandhalas. *Concepts Magn. Reson. Part B Magn. Reson. Eng.* **2004**, *23*, 16–25. [CrossRef]
11. Reif, F. *Fundamentals of Statistical and Thermal Physics*; International Student Edition; McGraw-Hill Kogakusha: Tokyo, Japan; London, UK, 1965.
12. Webber, J.; Welle, A.; Livadaris, V.; Andreev, A. Pushing the limits of NMR cryoporometry in polymers from nanometer to micron. *ChemRxiv* **2020**. [CrossRef]
13. Blu¨mler, P.; Soltner, H. Practical concepts for design, construction and application of halbach magnets in magnetic resonance. *Appl. Magn. Reson.* **2023**, *54*, 1701–1739. [CrossRef]
14. Webber, J.B.W.; Corbett, P.; Semple, K.T.; Ogbonnaya, U.; Teel, W.S.; Masiello, C.A.; Fisher, Q.J.; Valenza, J.J., II; Song, Y.-Q.; Hu, Q. An Nmr study of porous rock and biochar containing organic material. *Microporous Mesoporous Mater.* **2013**, *178*, 94–98. [CrossRef]
15. Korb, J.-P. Multiscale nuclear magnetic relaxation dispersion of complex liquids in bulk and confinement. *Prog. Nucl. Magn. Reson. Spectrosc.* **2018**, *104*, 12–55. [CrossRef] [PubMed]
16. Strange, J.H.; Rahman, M.; Smith, E.G. Characterization of Porous Solids By NMR. *Phys. Rev. Lett.* **1993**, *71*, 3589. [CrossRef] [PubMed]
17. Mitchell, J.; Webber, J.; Strange, J. Nuclear magnetic resonance cryoporometry. *Phys. Rep.* **2008**, *461*, 1–36. [CrossRef]
18. Petrov, O.V.; Furó, I. NMR cryoporometry: Principles; applications; potential. *Prog. Nucl. Magn. Reson. Spectrosc.* **2009**, *54*, 97–122. [CrossRef]
19. Webber, D.J.B.W. ORCID: 0000-0002-8967-4671 (2024). Available online: https://orcid.org/0000-0002-8967-4671 (accessed on 5 September 2024).
20. Morris, G.A.; Processing, N.M.D.; Lindon, J.C.; Tranter, G.E.; Koppenaal, D.W. *Encyclopedia of Spectroscopy and Spectrometry*, 3rd ed.; Academic Press: Cambridge, MA, USA, 2017; pp. 125–133. ISBN 9780128032244. [CrossRef]
21. Mnova NMR. Available online: https://mestrelab.com/software/mnova-software/nmr/ (accessed on 5 September 2024).
22. Garroway, A.N.; Grannell, P.K.; Mansfield, P. Image Formation using Nuclear Magnetic Resonance. U.S. Patent 4,021,726, 3 May 1977.
23. Strange, J.H.; Webber, J.B.W. Multidimensionally resolved pore size distributions. *Appl. Magn. Reson.* **1997**, *12*, 231–245. [CrossRef]
24. Webber, J.B.W. The Characterising of Porous Media. Ph.D. Thesis, University of Kent, Canterbury, UK, 2000. Available online: https://kar.kent.ac.uk/13453/ (accessed on 5 September 2024).
25. Webber, J.B.W.; Livadaris, V.; Andreev, A.S. USY zeolite mesoporosity probed by NMR cryoporometry. *Microporous Mesoporous Mater.* **2020**, *306*, 110404. [CrossRef]
26. Workman, M.J.; Webber, J.B.W.; Mukundan, R. Analysis of PEMFC electrode pore structure–bridging the mesoscale gap. In Proceedings of the 236th Meeting of the Electrochemical Society, Atlanta, GA, USA, 16 October 2019.
27. Bland, P.A.; Jackson, M.D.; Coker, R.F.; Cohen, B.A.; Webber, J.B.W.; Lee, M.R.; Duffy, C.M.; Chater, R.J.; Ardakani, M.G.; McPhail, D.S.; et al. Why aqueous alteration in asteroids was isochemical: High porosity does not equal high permeability, Earth and Planetary. *Sci. Lett.* **2009**, *287*, 559–568. [CrossRef]
28. Eisenman, H.C.; Nosanchuk, J.D.; Webber, J.B.W.; Emerson, R.J.; Camesano, T.A.; Casadevall, A. Microstructure of cell wall-associated melanin in the human pathogenic fungus cryptococcus neoformans. *Biochemistry* **2005**, *44*, 3683–3693. [CrossRef] [PubMed]
29. Alam, M.; Okonkwo, C.; Cachaneski-Lopes, J.; Graeff, C.; Batagin-Neto, A.; Tariq, S.; Varghese, S.; O'connor, M.; Albadri, A.; Webber, J.; et al. Date fruit melanin is primarily based on (−)-epicatechin proanthocyanidin oligomers. *Sci. Rep.* **2024**, *14*, 4863. [CrossRef] [PubMed]
30. Bruker—Minispec. Available online: https://www.bruker.com/en/products-and-solutions/mr/nmr-epr-td-nmr-industrial-solutions/minispec-mq-series.html (accessed on 5 September 2024).
31. Oxford Instruments—MQC+. Available online: https://nmr.oxinst.com/mqc (accessed on 5 September 2024).
32. Resonance Systems—Spin Track. Available online: www.nmr-design.com (accessed on 5 September 2024).
33. Turbospec LLC—Turbospec—e400. Available online: http://turbospecllc.com/ (accessed on 5 September 2024).
34. Lab-Tools Ltd.—Mk4 & MK5. Available online: https://nmrspectrometer.lab-tools.com/ (accessed on 5 September 2024).
35. Oxford Instruments—MQR. Available online: https://nmr.oxinst.com/mqr (accessed on 5 September 2024).
36. Oxford Instruments—GeoSpec 2 & 12. Available online: https://nmr.oxinst.com/campaigns/geospec (accessed on 5 September 2024).

37. LexMar Global Inc.—Mag Station. Available online: https://lexmarglobal.com/magstation-ii (accessed on 5 September 2024).
38. LexMar Global Inc.—MagModule. Available online: https://lexmarglobal.com/magmodule-ii-1 (accessed on 5 September 2024).
39. Stelar, s.r.l. SMARTracer—FFC NMR Relaxometer. Available online: https://www.stelar.it/products/smartracer (accessed on 5 September 2024).